INSTYTUT FIZYKI JĄDROWEJ
im. Henryka Niewodniczańskiego
Polskiej Akademii Nauk
ul. Radzikowskiego 152, 31-342 Kraków

www.ifj.edu.pl/publ/reports/2015/

Kraków, grudzień 2015

Raport Nr 2084/AP

MULTIMODAL APPROACH FOR IONIZING RADIATION DAMAGE INVESTIGATION

W.M. Kwiatek, J. Adamczyk, J. Bobrowska, A. Borkowska, M. Lekka, J. Lekki, E. Lipiec, J. Miszczyk, J. Pabijan, Cz. Paluszkiewicz, A. Panek, N. Piergies, K. Pogoda, Sz. Prauzner-Bechcicki, L. Quaroni, M. Roman, A. Wiecheć, J. Wiltowska–Zuber

REGIONAL PROGRAMME NATIONAL COHESION STRATEGY
Małopolska KRAKÓW Region
EUROPEAN UNION EUROPEAN REGIONAL DEVELOPMENT FUND

Abstract

The new, leading edge laboratory has been established and put into routine operation. The laboratory is focused on multimodal studies of the cellular response to ionizing radiation and provides support and research facilities for the Bronowice Cyclotron Centre. Spectroscopic imaging of cells and tissues (examining in particular the internal structure of cells, the cytoskeleton organization, cells' mechanical and biochemical properties), as well as research at the molecular level, has been applied in research for the purpose of searching new strategies of prevention and therapies of cancer and other pathologies and in fundamental research in the field of structural and vibrational analysis of condensed matter.

The multimodal approach, illustrating the full laboratory potential, has been applied to radiation effect studies of transitional cells – human bladder carcinoma cells (T24 cell line). Cells were irradiated with three X-ray radiation doses: 1 Gy, 3 Gy, and 10 Gy and subsequently studied using all instruments of the new laboratory. The presented results demonstrated that the AFM elasticity measurements can be applied to quantitatively estimate alterations induced upon X-ray irradiation at the single cell level. A combination of AFM and InfraRed Spectroscopy (NanoIR2 setup) was successful in characterization molecular changes occurring in the nuclear environment following cellular irradiation. Particularly useful information acquired was the observation of changes in distribution of macromolecules with a spatial resolution at the level of the single organelle. The observed changes correlate with radiation dose and thus may become a tool for studying the biological effects of radiation exposure. The application of Raman microspectroscopy for radiation-induced damage investigations provided detection of such spectral changes as strand breaks, base unstacking, and DNA conformational transformations. These studies give crucial information about the damage associated with irradiation and cellular response for radiation dose at single cell level. Moreover, Raman spectroscopy provides possibility to investigate structural changes present within the same sample. Complementary UV–VIS technique, on the basis of γ-H2AX test, delivered quantitative data of radiation damage, manifesting in presence of double strand breaks in DNA in 1st and 2nd day of culture (1 hour and 24 hours after irradiation).

Introduction

Ionizing radiation from natural radioactivity, from outer space, and resulting from human activity and technology constitute a heterogeneous field covering the whole living area of the human population. A huge effort has been undertaken in last decades in order to study the biological effects and to estimate risk related to exposure to radiation [Tubiana 2005]. These studies are carried out at many levels and timescales, extending from the assessment of energy deposition at the molecular level, through bio-molecular damage and its repair mechanism researches, up to examination of the irradiation consequences for the living cell and tissue.

Medical diagnosis process requires medical imaging at scales ranging from single molecules through cells, tissues, organs, and up to a whole body. In collaboration with medical partners, the newly emerging imaging modalities based on the focused beams of different radiations (infra-red, X, nuclear) are developed [Folkard 2001, Folkard 2006, Gerardi 2006, Imaseki 2007, Bożek 2009, Lekki 2014, Adjei 2015] as complementary methods to those well established and commonly used in medical practice. We shall concentrate on developing the best methods of imaging required for the understanding, screening, and therapy of cancer and other major diseases.

Ionizing radiation mostly induces damage in the genomic DNA what is the basic source of signal generation. Parallel to direct effects following the energy deposition along the radiation track [Nikjoo 1998], several second order, non-targeted effects appear [Nagasawa 1999, Nuta 2008, Lipiec 2015]. Newly created reactive oxygen species (ROS) inactivate phosphatases and result in activation of kinases localized at the plasma membrane following ligand-independent activation of receptor kinases. Thus, cells show elevated radiation sensitivity in order to dysfunction of some specific enzymes crucial for checkpoint control. The dynamic balance between DNA damage repair systems, and the interplay between proteins participating in reconstruction define the cell death type. In some cell types (i.e. malignant cell lines), however, the DNA restoration mechanisms are drastically changed; multifarious signals decide to what extent the repair of radiation-inflicted damage is sustained or arrested.

The above considerations lead to the conclusion that in investigations of the cellular response to ionizing radiation multimodal approach is highly recommended. Therefore the project of setting up new modern laboratory has been erected.

Goals of the project:

Creation of a modern region-wide laboratory, capable of carrying out unique research on the impact of ionizing radiation on living organisms and providing research facilities for the Bronowice Cyclotron Centre.

Conducting research, using physical methods, for the purpose of eradication cancer and other pathologies. This includes spectroscopic imaging of cells and tissues (examining the internal structure of cells, the cytoskeleton organization, cells' mechanical and biochemical properties) as well as research at the molecular level.

Carrying out fundamental research in the field of structural and vibrational analysis of condensed matter.

In order to achieve the above goals the Laboratory has been equipped with the following, main research systems and devices:

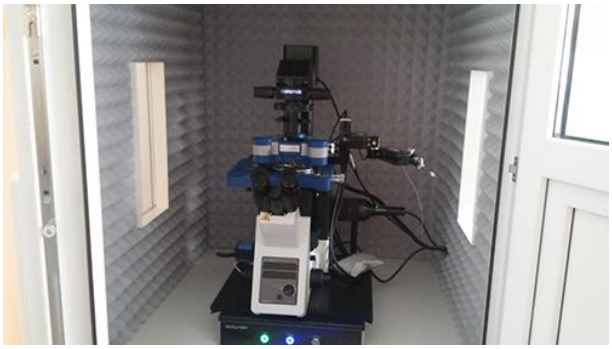

Figure 1. *Atomic force microscope integrated with a fluorescent microscope (nanoWizard 3, JPK).*

Figure 2. *The integrated Raman-AFM system capable of performing Raman microspectroscopy, atomic force microscopy (AFM) and Raman nanospectroscopy enhanced on the AFM tip (TERS).*

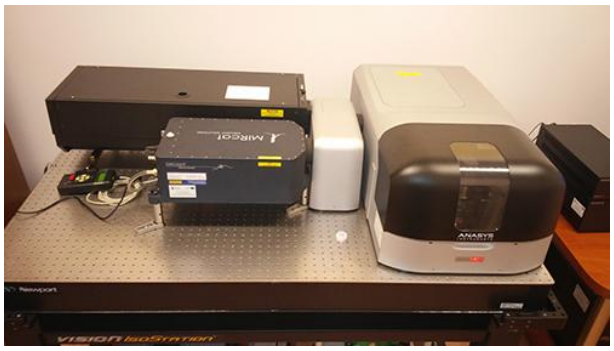

Figure 3. *The NanoIR system - Integrated IR-AFM layout - infrared microscope with nanometer resolution achieved by enhancing signal on the AFM tip.*

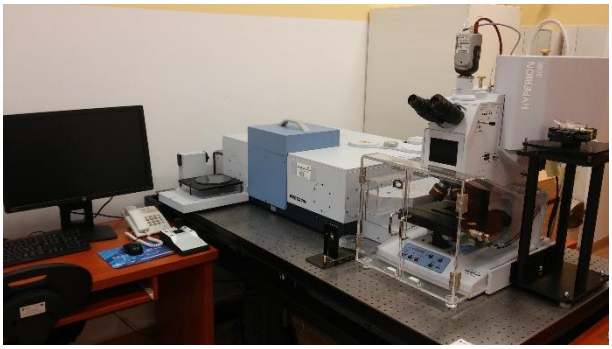

Figure 4. *Vacuum FTIR spectrometer (VERTEX 70 FT-IR spectrometer with the HYPERION 3000 microscope) , bolometer and FPA detector. Operation range: form near to far infrared. Purpose: taking chemical characteristics of the sample, including studies of radiation damage to cells and tissues, and interaction with chemotherapeutic agents.*

Figure 5. *Independent fast imaging IR microscope (Nicolet IN10 MX) – for spectral imaging and spot measurements, equipped with three detectors and motorized microscope table. Capable of recording the spectrum in both transmission and reflection modes, as well as of taking classical microscope images of the sample.*

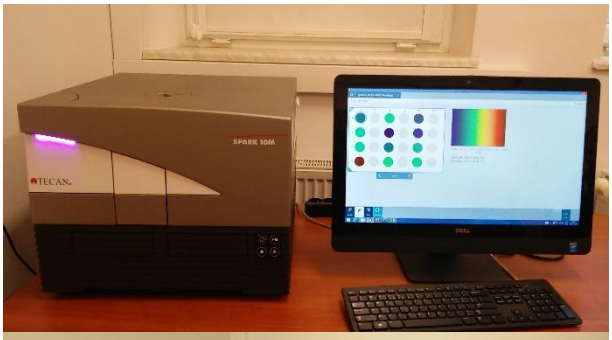

Figure 6. *UV-VIS Spectrometer - plate reader – (spectrophotometer Spark M10), allowing the use of multiple absorption, fluorescence and luminescence markers.*

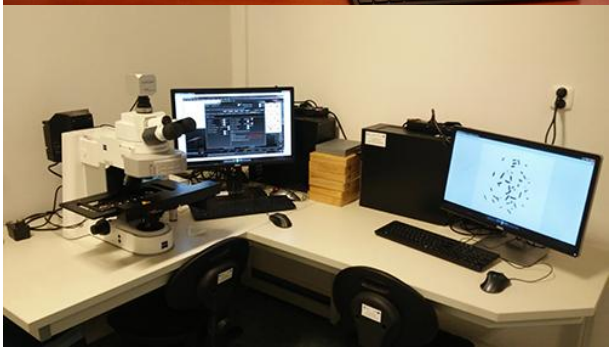

Figure 7. *System for automatic analysis of chromosome aberrations. Upgrading our existing system (Zeiss microscope AxioImager Z2) for karyotype determination. The extension includes capability of automatic metaphase searching for accreditation requirements and building up a test stand of GTG and FISH analysis.*

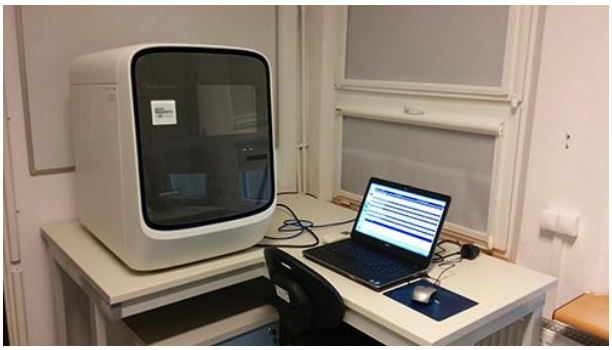

Figure 8. *The RT-PCR system for real-time testing of DNA sequence. Research involved: gene expression studies, single nucleotide polymorphism (SNP) searching, dysfunctional copy number of the gene (CNVs), µRNA profiles, detection of pathogens.*

Experiment description

In order to show the integrity and complementary approach for cells and tissues studies the available techniques at the Laboratory of spectroscopic imaging for radiobiology, treatment and research of complex systems at the Institute of Nuclear Physics, Polish Academy of Sciences in Krakow have been applied to selected cell line and tissue. The general aim of the studies was to evaluate changes in: mechanical properties, chemical composition and local structure of single cells induced by X-ray irradiation. In addition, the evaluation of changes in tissues due to selected diseases were a subject of these studies.

Materials and Methods

Cell line. Cancer cells, originating from transitional cell carcinoma, (T24 cell line) were cultured in a RPMI 1640 medium (Sigma) supplemented with 10% fetal bovine serum (FBS, Sigma). They were grown in culture flasks (Sarstedt) in a CO_2 incubator (Nuaire) providing 37ºC and 95% air/5% CO_2 atmosphere. For selected measurements T24 cells were grown to adherence on round CaF_2 optical windows (25 mm x 1 mm). The relative humidity was kept above 98%. For all, planned measurements, they were trypsinized using a 0.25% trypsin-EDTA solution (Sigma) for 2 minutes and moved into glass coverslips.

For nanoIR, Raman, and FTIR experiments cell fixation was performed within 1 hour from irradiation according to the following procedure. Initially, culture medium was removed and replaced by phosphate buffered saline (PBS, Sigma). Then cells were fixed using 3.7% paraformaldehyde in PBS for 10 minutes. The surplus fixative was washed away using PBS (2 x 2min). Subsequently, PBS was replaced by PBS diluted 1:1 in deionized water (dH_2O, Cobrabid purification system, 0.08 µS) dH_2O and incubated for 2 minutes. This step was done in duplicate in order to gently lower the salts concentration within the cells. Finally cells were washed in dH_2O and air dried for at least 1 hour prior to the measurement. All the steps were carried out at room temperature. Fixed cells were allowed to air dry for at least 24 h on the CaF_2 slides.

X-ray treatment. Seeded cells were divided into 4 groups and, after a period of at least one day, three groups were irradiated with X-rays from the X-Ray Machine MG325 (250 kV, 10 mA). The fourth group was not irradiated and was treated as control. First group of cells was irradiated with the dose of 1 Gy, the second one with dose of 3 Gy and the third one with the dose of 10 Gy. In each case the dose rate was 2.1 Gy/min.

Fluorescent staining. The cells grown on glass coverslips were washed three times with the PBS buffer. Next, the cells were fixed by adding a 3.7% paraformaldehyde solution in PBS buffer (for 20 minutes, and then, they were washed with PBS buffer for 5 minutes. Afterwards, the cell membrane was permeabilized by incubating the cells with a 0.2% Triton X-100 (Sigma) in PBS solution for 5 minutes at 4°C. Then, cells were rinsed three times with PBS buffer. Such prepared coverslips with cells were fluorescently labelled in a humidity chamber. A 400 µl of a solution containing phalloidin labelled with Alexa Fluor 488 (Molecular Probes, 0.33 µM) was added for 30 minutes. After this time, coverslips were washed with the PBS buffer and immediately imaged under fluorescent microscope.

Fluorescence microscopy. The fluorescence microscopy was carried out using an Olympus IX71 inverted microscope (Olympus, Japan) equipped with a X-Cite® 120Q LED light source system (uniformly illuminating the whole sample area) and U-MNB2 filter used for actin filaments (Alexa Fluor 488) visualization. For image recording, a XC10 digital camera was applied. The camera provides a 1376 x 1032 pixel (1.4 million) image with a 2/3 inch optical format. Images were recorded using the CellSens Dimension program (Olympus Corp.).

Atomic force microscopy. The atomic force microscopes used for the elasticity measurements were a XE120 model (Park Systems, Korea) and NanoWizard 3 (JPK, Germany). Both AFM's are integrated with the inverted optical microscope equipped with fluorescent functionality. The AFM are equipped with a "liquid cell" enabling the measurements in liquid conditions close to natural ones. Elasticity measurements were carried out using AFMs working in contact mode. The commercially available silicon nitride cantilevers (PNP-TR from NanoWorld) were used. The spring constants were verified based on thermal excitations of a free end of a cantilever [Sader 1999]. The calculated, corresponding spring constants were 0.049 N/m.
To estimate the elastic properties of the investigated samples, so called force curves were recorded. A force curve is a dependence between the cantilever deflection and relative scanner position that is later converted into force versus distance curve. In elasticity measurements, force curves are usually recorded on both calibration, reference and cells' samples. A reference curves is used for photodetector sensitivity calibration since it reveals linear dependence between the cantilever deflection and the piezoscanner extension. A curve recorded on a single cell revels non-linear behavior due to indentation effect. The curves were acquired in 36 different positions recorded within a scan area of 6 μm × 6 μm. The measurements were carried out on a cell close to its center (a nucleus region). The curves were acquired with an approach speed of 8 μm/s.

Quantitative imaging. The quantitative imaging mode was provided by the NanoWizard 3 (JPK). It enables to study the distribution of mechanical properties with high spatial resolution. The commercially available silicon nitride cantilevers (PNP-TR from NanoWorld) were used. The spring constants were verified based on thermal excitations of a free end of a cantilever [Sader 1999]. The calculated, corresponding spring constants were 0.026 N/m. Stiffness maps were recorded over the scan area of 250 μm^2, on which a grid of 64 × 64 points was set. The approach speed was set to 8 μm/s.

Elasticity of cells. The difference between force curves recorded on hard glass and on soft cell surfaces enables to determine the force versus indentation curves [Lekka 1999, Lekka 2012), which is the basis for the calculations of the elastic modulus. The elastic modulus (i.e. the Young's modulus) was determined from the Hertz-Sneddon model assuming that the indenting AFM probe has a conical shape, described by the open angle of 70°. The final modulus value was represented as a mean ± standard deviation (for n = 15 cells).

NanoIR – Atomic Force Microscopy combined with InfraRed spectroscopy. AFM-IR imaging was performed on nanoIR2 system (Anasys Instruments, CA, USA) by recording the photothermal response of the sample while scanning in contact mode and exciting the sample at a fixed wavelength. The laser power was set at 17% of maximum for excitation. 8 measurements were co-added for each spatial position. The parallel AFM contact mode measurement is performed using a scan rate of 0.5 Hz, a resolution of 256 pixel in the X and Y direction, and turning on the feedback loop of the Z scanner. The setpoint value was defined by an automated

algorithm for each sample and P and I gains were set at 1 and 0.5 respectively. Samples were first inspected by AFM imaging, using both height and deflection images. Single IR photothermal spectra were recorded on specific cellular locations by scanning the excitation laser over the desired wavelength range and recording the photothermal response via the deflection response of the AFM tip. Spectral scans were performed over the 1000 – 1800 cm^{-1} and 2700 – 3000 cm^{-1} spectral intervals using 1 cm^{-1} steps. An OPO laser was used as the excitation source with power set at 16% of the maximum for all spectral scans. The photothermal induced deflection of the tip is measured by the movement of a laser beam reflected by the cantilever and recorded by a four quadrant detector as a free induction decay signal (FID). The resonance spectrum of the cantilever is extracted from the FID using a Fast Fourier-Transform algorithm. The resonance at approximately 200 kHz is selected via a Gaussian filter with a half-width of 50 kHz and its intensity plotted as a function of wavelength and divided by a background spectrum of the laser to provide an infrared absorption spectrum of the sample. Alternatively the maximum peak-to-peak amplitude of the FID was plotted as a function of wavelength and divided by the background spectrum of the laser, to provide an alternative representation of the infrared absorption spectrum of the sample. The signal-to-noise ratio was improved by co-adding 1024 measurements per spectral step in the sample measurement and 2048 measurements per spectral step in the background spectrum. The background spectrum was obtained by averaging three successive spectra to reduce laser fluctuations.

Raman spectroscopy. The Raman spectra were collected using inVia Renishaw spectrometer. The spectrometer is equipped with a confocal microscope Leica in combination with immersion objective with the 63x magnification (live cells) and air objective with the 50x magnification (fixed cells) as well as EMCCD detector. As an excitation source the laser with the 632.8 nm line with exposure time of 20 sec and 10 accumulations, was used. The 100% of laser power during the measurements, was applied.

UV-VIS (UV – Visual) spectrometry. A plate reader – spectrophotometer Spark M10 was used for a) automated cell counting, b) cytotoxicity LDH test (absorbance measurements), and c) γ H2AX foci assay (fluorescence of DSBs -stained with Texas Red and nuclei – stained with DAPI). The T24 non-irradiated and irradiated cells with X-rays at 1 Gy and 3 Gy dose were chosen for this study. The fourth group of cells (irradiated with 10 Gy) was not chosen due to high absorbance. The cells were seeded into 24-wells black plate. The density of cells was counted in two methods: a) in the Bürker hemocytometer under light microscopy (usually applied in our laboratory) and b) in automated cell counting under spectrophotometer.
Example of cells number measurements mages are shown below (Figures. 9, 10). The density of cells was ~ 8,000 cells/ml.

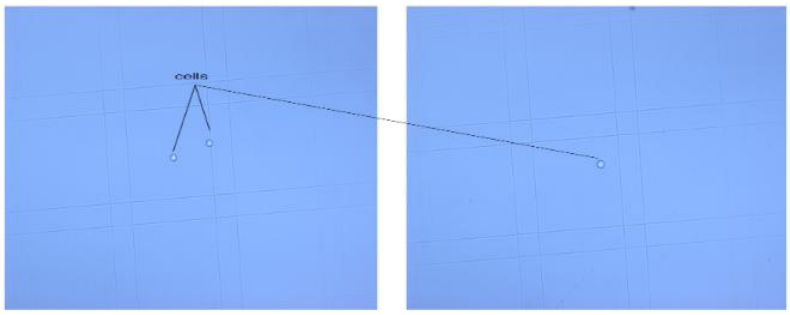

Figure 9. *T24 cells in the Bürker hemocytometer.*

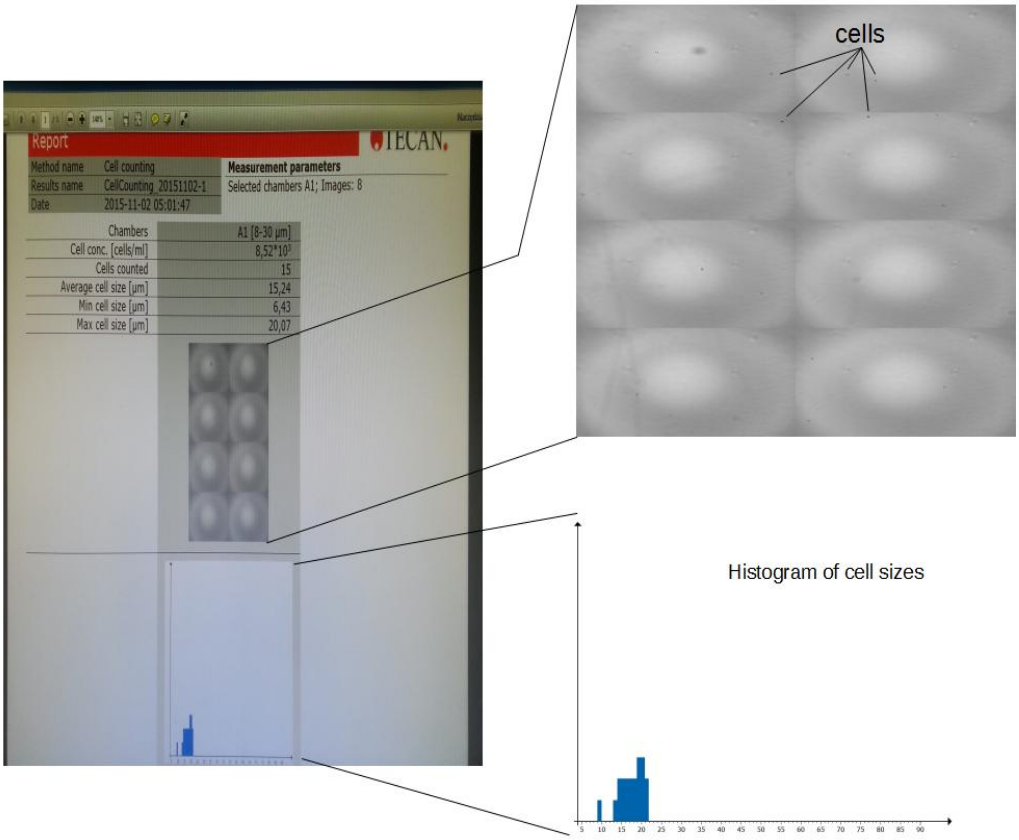

Figure 10. *Report from automatic cell counting.*

The cytotoxicity analysis

The LDH assay was conducted to examine the cytotoxicity of radiation treatment. LDH cytotoxicity assay (Clontech) is a reliable colorimetric assay to quantitatively measure lactate dehydrogenase (LDH) released into the media from damaged cells as a biomarker for cellular cytotoxicity and cytolysis [LDH 2007]. The medium from irradiated and non-treated cells were collected 1 hour and 24 hours after irradiation. The cytotoxicity analysis was performed according to following equation: Cytotoxicity[%]= (quadruple absorbance-low control)/(high control-low control) x 100%. The experiments were repeated twice.

The γ H2AX foci assay

The γ- H2AX foci were analyzed under spectrophotometer after conjugation with anti-γ H2AX monoclonal antibodies conjugated with fluorochrome. After X-ray exposure, the cells were incubated for 1 hour or 24 hours, washed with PBS (phosphate buffered saline) and fixed with 1.5% p-formaldehyde. They were then permeabilized (0.25% Triton X-100 solution in PBS) for 30 min at 4ºC, washed three times in PBS and incubated in a blocking buffer (5% fetal bovine serum in PBS) for 1 hour at room temperature. After the preparatory stage, the cells were first incubated with the anti-mouse anti-phospho-Histone H2AX (Ser139) antibody (Clone JBW301, Maus, Upstate, New York, USA) for two hours at room temperature, and thereafter with goat anti-mouse secondary antibody conjugated with TexasRed (Sigma-Aldrich,

Stenheim, Germany) for 1 hour at room temperature. The samples were washed twice in washing TBS buffer (Triton X-100 and BSA in PBS) [Ugenskiene 2007]. The mean value (± SD) from two repetitions was calculated. The result was presented as fluorescence measurement (in RFU-*relative fluorescence* unit) and also as percentage of γ- H2AX foci expressed after irradiation in relationship to control (non-treated).

MetaSystems

In the project the high-performance slide scanning Metafer platform from MetaSystems Company with Ikaros software (GmbH) was purchased for automatic scanning of slides and karyotyping of cytogenetic preparations. In the study of the biological effects of ionizing radiation we scanned a cytogenetic slide to acquire image database of metaphases from irradiated peripheral blood lymphocytes of healthy donors. Example of image from the acquired base is shown on Figure 11.

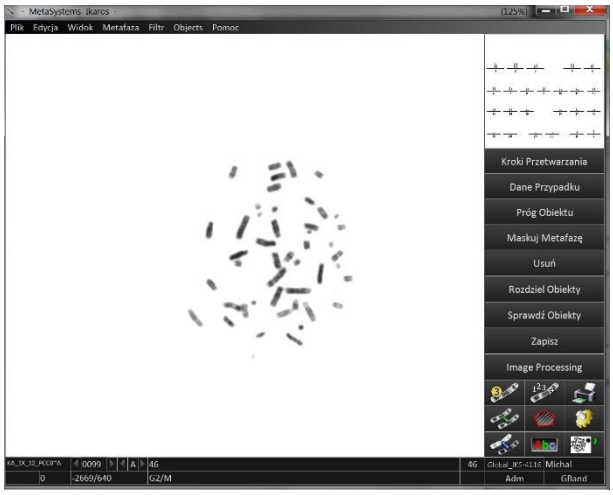

Figure 11. *Example of metaphase of human lymphocyte.*

Based on the picture of metaphase, the karyotype in both the number and structure of chromosomes was performed. Results of this process presented as metaphase karyotype is shown on Figure 12.

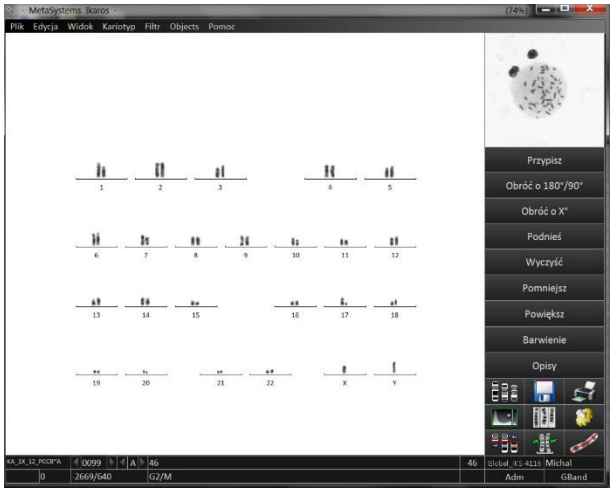

Figure 12. *Image of metaphase karyotype of lymphocyte exposed to ionizing radiation.*

RT-PCR (Real Time Polymerase Chain Reaction). In the project the QuantStudio ™ 7 Flex System (from Thermo Fisher) was purchased with two different block type: Fast 96 Well and 384 Well. In the first stage of the studies for both blocks were performed calibration standard curves for RNAse P. In 96 and 384 - well plates were placed respectively at 4 and 10 repetitions of a known quantity of copies of the gene, RNAse (standard) ranging from 1,250 copies to 20,000 copies. The remaining wells were given unknown concentrations of RNase P. After a two-step PCR reaction standard curves were obtained. The relation between a threshold cycle (C_T) and the concentration of the target sequence (number of gene copies) allows for a precise quantitation of the genetic material in the sample.

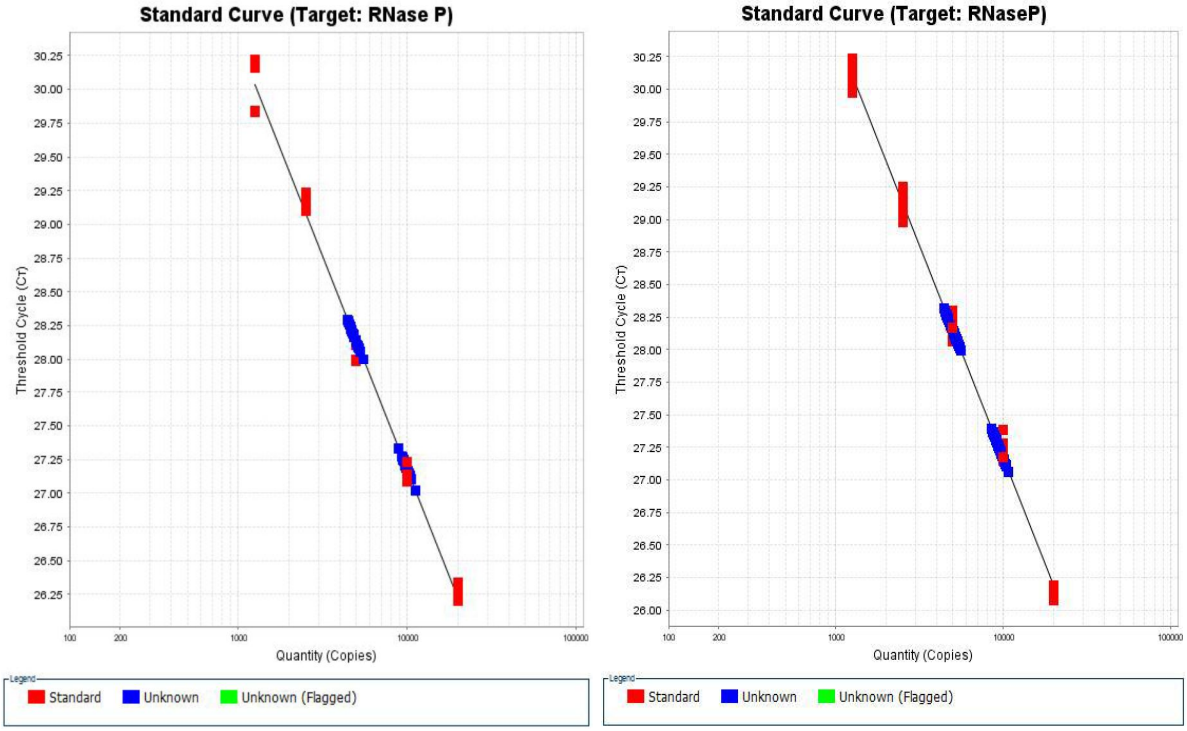

Figure 13. *Standard PCR curves.*
Left – slope: –3.167 Y-Intercept: 39.8431 R^2: 0.993 Eff%: 106.898
Right – slope: –3.2484 Y-Intercept: 40.1619 R^2: 0.996 Eff%: 103.163
C_T - the threshold cycle which is the cycle number (C), wherein detected fluorescence exceeds the threshold ($_T$)

Results

Actin filaments distribution.

The elastic properties are linked with the organization of actin filaments thus to visualize the effect of X-ray irradiation on living T24 cells, F-actin was labelled fluorescently using phalloidin conjugated with Alexa Fluor 488 dye. The F-actin distribution in irradiated cells changed as compared to control samples. Upon irradiation cells shrink and lost nice organization of long actin filaments bundles that was accompanied by membrane blebs observed at the cell's edges (Figure 14).

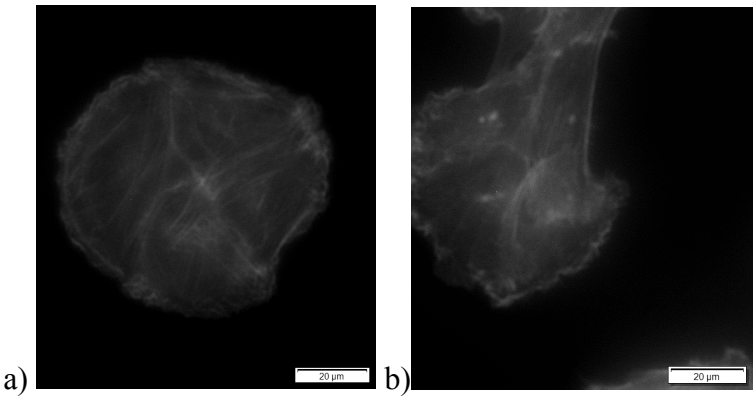

Figure 14. *F-actin distribution recorded for control sample (a) i.e. non-irradiated T24 cells and for (b) cells irradiated with X-ray with the dose of 10 Gy. Scale bar is 20 microns.*

Single cell elasticity and stiffness maps.

To evaluate changes induced by X-ray irradiation the elastic properties were quantified by the Young's modulus (Figure 15). Its value was calculated for two indentation depths i.e. 100 nm and 500 nm. These two values correspond to mechanical response of membrane- and cytoskeleton-dominated regions, respectively.

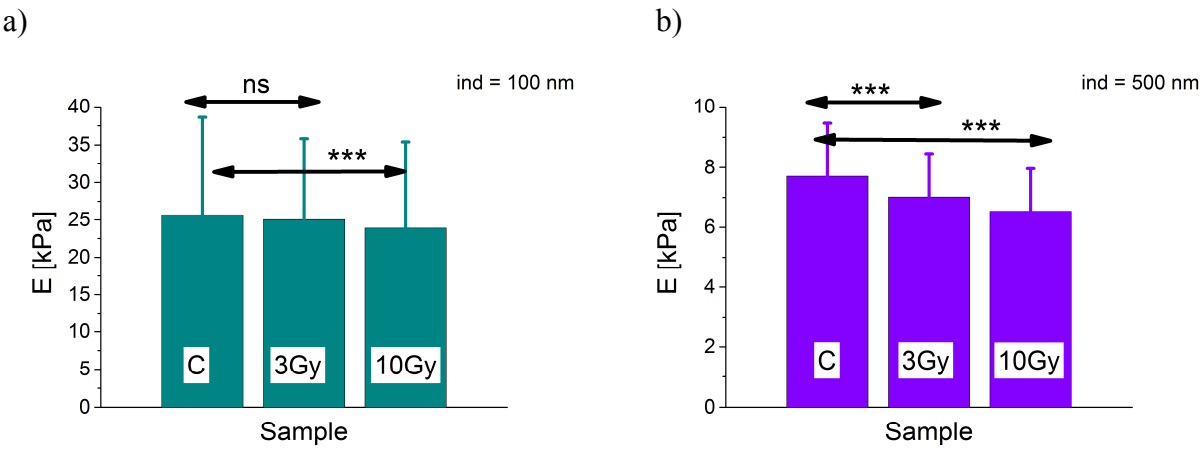

Figure 15. *Single cell elasticity quantified by the Young's modulus calculated for two indentation depths of (a) 100 nm and (b) 500 nm. The modulus represents a mean ± standard deviation (calculated for n = 15 cells)*

For the indentation of 100 nm, the Young's modulus values were associated with large standard deviations what denotes large mechanical variability of the superficial layers of the cells. It described the regions rich and poor in the network of actin filaments. For large indentation of 500 nm, the modulus denotes the overall stiffness of a whole cell, which is accompanied by the decrease of the modulus value. The X-ray irradiation induces the reorganization of F-actin within a cell in a dose- and indentation-dependent manner.

The obtained stiffness maps at the indentation depth of 100 nm correspond to a surface layer of a cell composed mainly of membrane but having a contribution of underlying F-actin cortex. Probing superficial layers by quantitative imaging (QI) delivers the detailed information on mechanical variability of such a layer (Figure 16).

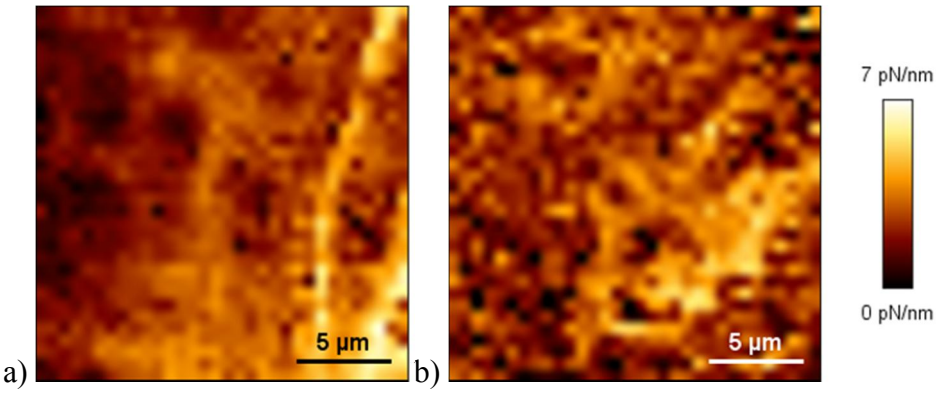

Figure 16. *Stiffness maps recorded for (a) control (non-irradiated) T24 cells and (b) and cells irradiated by X-rays with dose of 10 Gy.*

The non-irradiated cells showed long fibres with larger stiffness what corresponded to the F-actin filaments underlying beneath cell membrane. After irradiation, they vanished what manifested in both lower Young's modulus values.

FTIR microspectroscopy

Fixed and dried T24 cells on CaF_2 optical windows were moved to the stage of the Hyperion microscope and measured in air, without purging. Single cell microspectroscopy measurements were performed by imaging an extended portion of the sample using the Hyperion visible camera and marking the cells selected for investigation. The marked cells were measured automatically and sequentially using the following instrumentation parameters. The Vertex interferometer was setup for measurements in the mid-IR region using a KBr-supported Ge-multilayer beam splitter and a thermal source. The interferometer was scanned at 40 kHz while setting the source aperture at 6 mm in size. Light focusing on the sample and collection were performed using the optics of the Hyperion microscope fitted with a 15x Schwarzschild reflective objective and a LN_2-cooled mercury cadmium telluride (MCT) detector. Absorbed light was measured in a transmission geometry setting the downstream confocal aperture at 65 x 65 μm^2. 256 scans were performed per cell using 4 cm^{-1} spectral resolution. The interferograms were converted to the corresponding spectral domain data by using an FFT algorithm with a Blackman-Harris 3-Term apodization function, a Power Spectrum phase correction method and a zero filling factor of 2. Spectra were initially measured over the 350 – 7000 cm^{-1} range and plotted on an absorbance scale. Spectra were corrected for atmospheric absorption, restricted to the 900 – 4000 cm^{-1} interval and converted to their second derivative while also using a 9-point Savitzky-Golay smoothing algorithm. Instrumentation control, data collection and data preprocessing were performed using the software OPUS 7.5 from Bruker.

Principal Component Analysis (PCA) and Sample Classification

Principal Component Analysis and Sample Classification were performed using the software The Unscrambler X, from CAMO. Second derivative traces of single cell spectra were imported as matrices of comma separated values. For PCA analysis, the traces were restricted to the 900–1340 cm^{-1} and 2750–3150 cm^{-1} spectral ranges. PCA classification was performed on mean centered data using the NIPALS algorithm and 7 principal components, tested by the cross validation method and defined outliers as having a leverage limit of 3.0. Results are represented as scatter plots for pairs of principal components. PCA analysis was repeated three times for each spectral range separately. After a first analysis, outliers were excluded and the remaining dataset was used for a subsequent PCA analysis. This cycle was repeated a second time to exclude additional outliers. The results of the third cycle of classification are discussed in the following section.

Figure 17 shows the average single cell FTIR spectra for the three different exposures in the 2750-3200 cm^{-1} spectral range and in the 900-1430 cm^{-1}, together with the corresponding second derivative traces. Comparison of the spectra in the higher frequency region shows a clear decrease in absorbance for the bands at 2854 cm^{-1} and 2921 cm^{-1} following irradiation. In contrast, changes in average spectra in the lower frequency region show only minor differences induced by irradiation, the most obvious ones being in the 1340 cm^{-1} region and in the 1080-1090 cm^{-1} region. Analysis of average spectra is by itself insufficient to clearly distinguish patterns of spectroscopic changes caused by irradiation. More informative conclusions can be obtained by performing a PCA analysis of single cell spectral data.

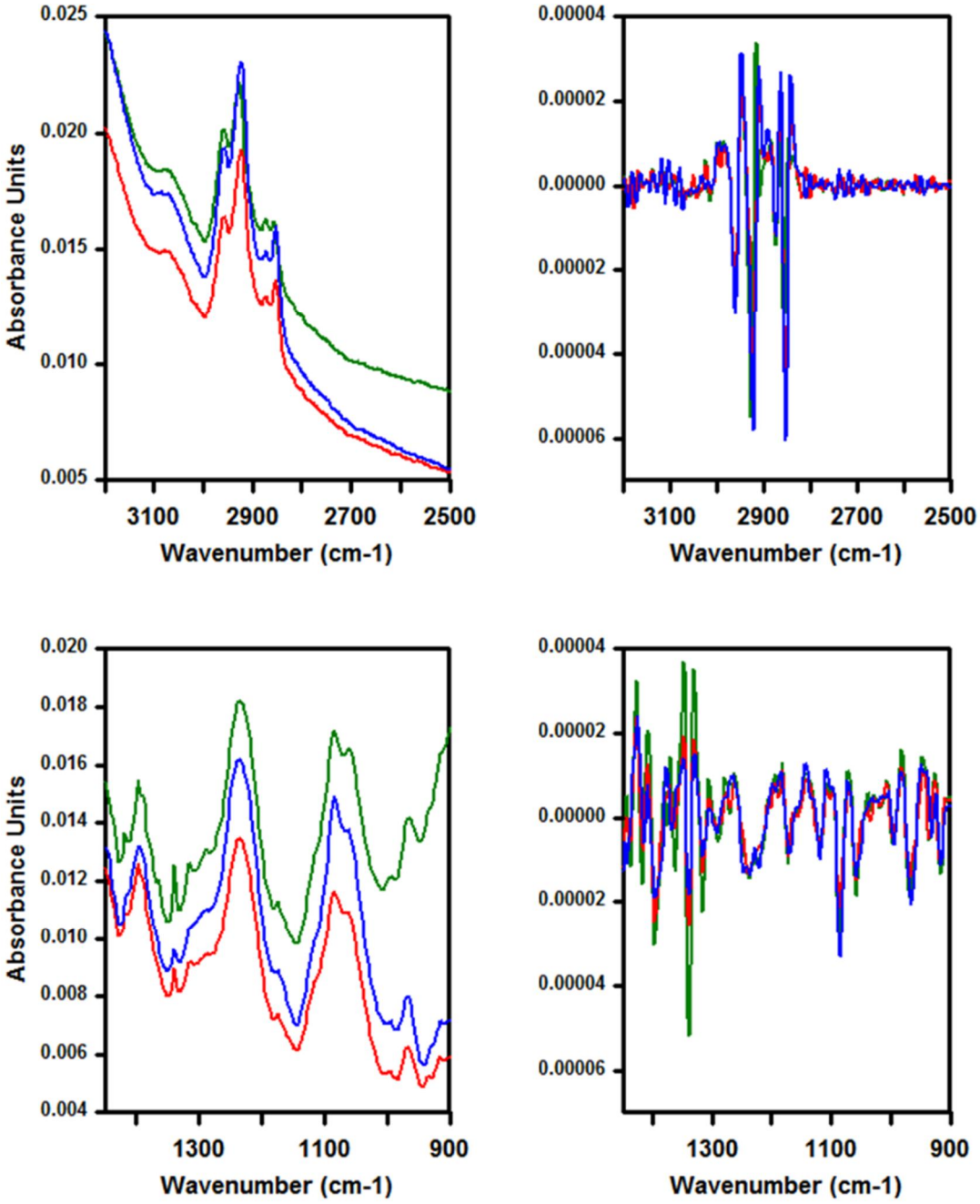

Figure 17. *Averaged single cell FTIR spectra.* ***a****: Absorbance spectra in the 2750–3200 cm^{-1} spectral range.* ***b****: Second Derivative of absorbance spectra in the 2750–3200 cm^{-1} spectral range.* ***c****: Absorbance spectra in the 1340–900 cm^{-1} spectral range.* ***d****: Second Derivative of absorbance spectra in the 2750-3200 cm^{-1} spectral range. Blue - control. Red – 3 Gy irradiated cells. Green – 10 Gy irradiated cells.*

Figure 18 shows the results of a PCA analysis performed on the 2750–3150 cm^{-1} spectral range of the samples. Pairwise scatter plots (panels a-e) of the scores show a clear clustering into three groups, corresponding to the three different samples. A comparison of the impact of the different principal components, shows that PC1 (panel f) and PC2 (panel g) account for most of the discrimination. The loadings of PC1 indicate that this component is dominated by absorption

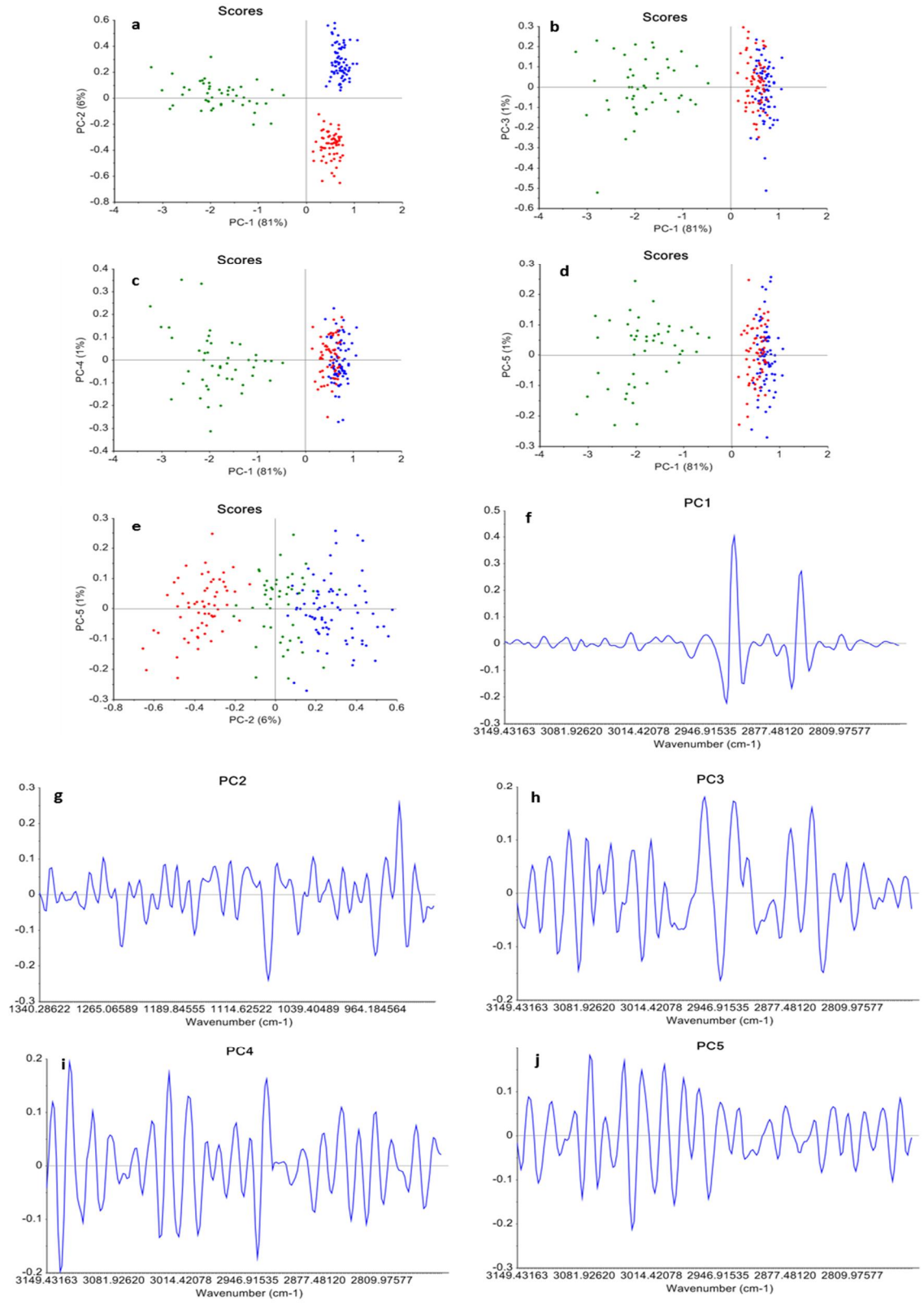

Figure 18. *PCA analysis performed on the 2750–3150 cm^{-1} spectral range.* ***a-e:*** *scatter plots of the scores for the sample set. Blue circles: control. Red circles: 3 Gy irradiated cells. Green circles: 10 Gy irradiated cells.* ***f-j:*** *loadings of the first five components.*

at 2854 cm^{-1} and 2921 cm^{-1}. These spectral positions in cellular spectra are dominated by the absorption of methylene groups in long chain alkyl groups, such as present in phospholipids, sphingolipids and triglycerides. The loadings of PC2, in contrast, show that the component is dominated by weaker absorptions at 2800 cm^{-1}, 2880 cm^{-1}, and 2946 cm^{-1}, suggesting a contribution from methyl groups and carbon-hydrogen single bonds. Overall the spectral differences between the samples can be ascribed mostly to changes in the composition of the lipid pools of the cells, in agreement with other experiments.

Figure 19 shows the results of a PCA analysis performed on the 900–1340 cm^{-1} spectral range of the samples. Pairwise scatter plots (panels a-c) of the scores show a clear clustering into three groups for this spectral range too. Also in this case PC1 (panel d) and PC2 (panel e) account for most of the discrimination, although a contribution is observed also from PC3 and PC4. The loadings of these components indicate overall contributions from absorption in the proximity of 975 cm^{-1}, 1085 cm^{-1}, 1095 cm^{-1}, 1250 cm^{-1} and 1340 cm^{-1}, plus a wealth of minor contributions. Most of these regions correspond to absorption from a variety of phosphate containing molecules, including nucleic acids, nucleotides, and phosphoproteins. The contribution at 1340 cm^{-1} is at the limit of the spectral region used for the classification, nonetheless it is a fairly strong contribution. One tentative assignment is to the side of the absorption of the bicarbonate ion, the intracellular concentration of which is expected drop as a consequence of acidification. These spectral changes are all in agreement with our current understanding of cellular processes triggered by radiation exposure, including protein synthesis, damage to the nucleic acid complement and acidification.

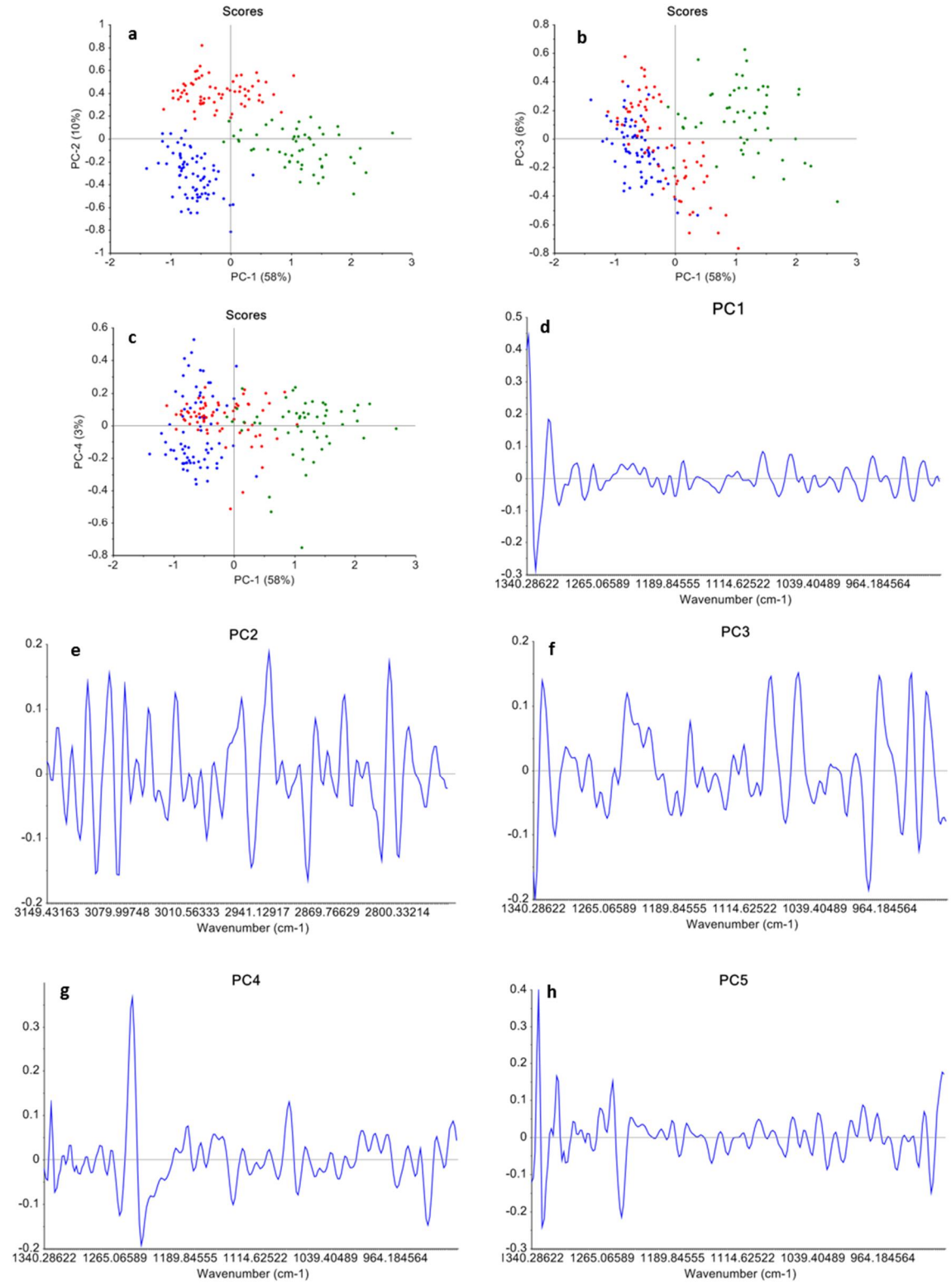

Figure 19. *PCA analysis performed on the 900–1340 cm^{-1} spectral range.* ***a-c:*** *scatter plots of the scores for the sample set. Blue circles: control. Red circles: 3 Gy irradiated cells. Green circles: 10 Gy irradiated cells.* ***d-h:*** *loadings of the first five components.*

In another study, the nanoIR spectra of individual nucleoli were recorded for T24 cells from samples irradiated with 10 Gy, 3 Gy and non-irradiated (control). Figure 20 shows typical IR photothermal spectra recorded for each sample.

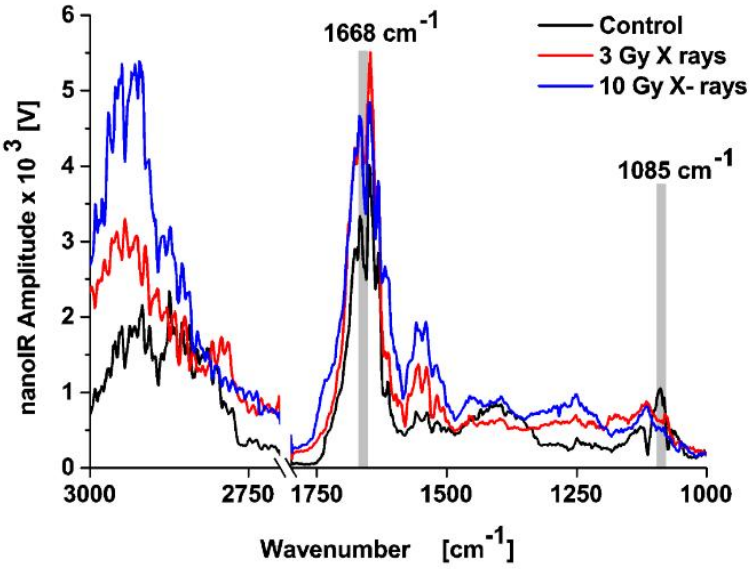

Figure 20. *IR photothermal spectra recorded from the nucleoli of T24 cells irradiated at different dose levels. Peak labels correspond to the bands used for AFM-IR imaging.*

The spectra display a large contribution from atmospheric water vapor, caused by varying humidity levels in the room that affects laser throughput through the optical train. This interference makes it difficult to appreciate fine spectral changes in the 1400–1800 cm^{-1} spectral region. Nonetheless major absorption changes can still be appreciated, as described later.

The main differences between irradiated and non-irradiated cells are observed in the spectral region between 1500 and 1700 cm^{-1}, dominated by absorption from Amide I and Amide II bands and nucleic acid C=O and C=N bonds, in the region between 1000 and 1200 cm^{-1}, dominated by nucleic acid, phospholipid and polysaccharide absorptions, and in the region between 2800 and 3000 cm^{-1}, characteristic of C–H group vibrations. Absorption in the 1500–1700 cm^{-1} range appears to increase following irradiation. In contrast absorption in the 1000–1200 cm^{-1} range shows formation of different absorption multiplets. Overall these changes can be attributed to protein synthesis in response to irradiation, leading to increased levels of RNA and polypeptide in the proximity of the nucleus [Criswell 2013]. The strongest change is observed in the CH stretching region (2800–3000 cm^{-1} interval), where a major increase in absorption from C–H and CH_3 groups tracks radiation dose. This change could also be attributed to a change in the lipid complement of the cell, an increase in both protein and RNA synthesis and also DNA methylation [Lipiec 2014].

To confirm this hypotheses we have performed AFM-IR imaging using the absorption bands at 1668 cm^{-1} and 1085 cm^{-1} to generate contrast. The results of these measurements for individual cell nuclei are shown in Figure 21.

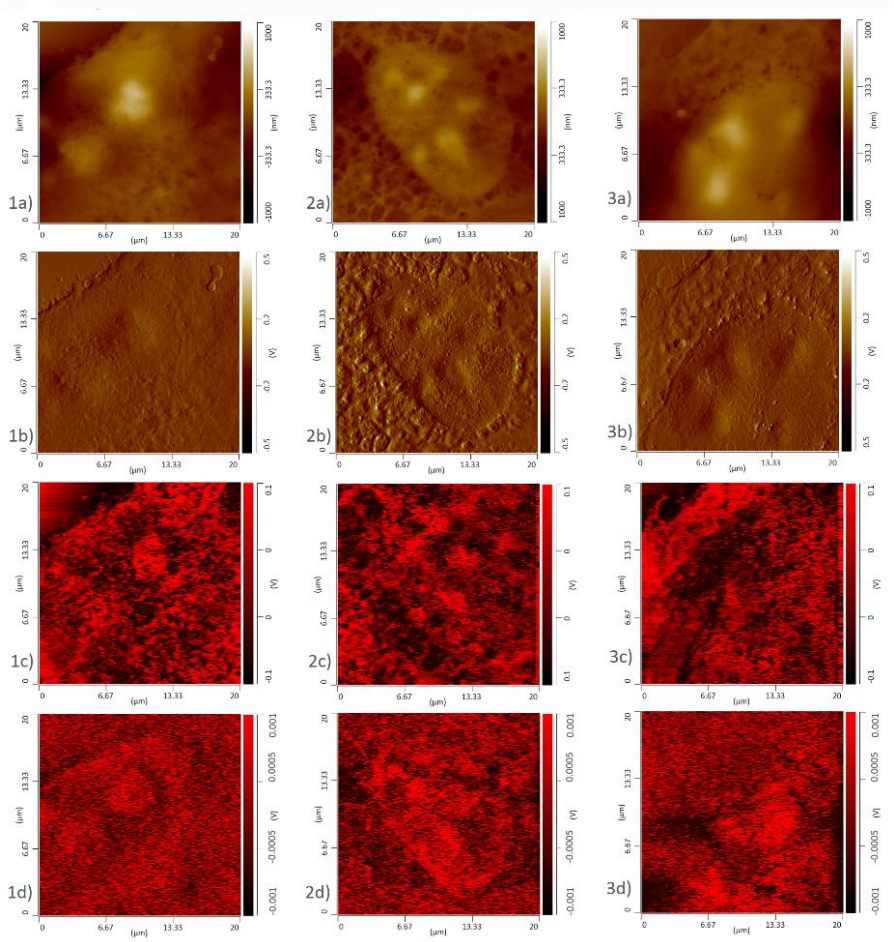

Figure 21. *AFM and AFM-IR images of nuclei of T24 cells irradiated at different dose levels. Column 1 – Control; Column 2 – 3 Gy; Column 3 – 10 Gy;*
Row a – Height AFM maps; Row b – Deflection AFM maps; Row c – IR maps at 1668 cm^{-1}; Row d – IR maps at 1085 cm^{-1}.

IR maps 1c and 1d show a distribution of absorption that correlates well with the AFM images of the nucleus. The nucleoli can be easily identified, as well as the nuclear envelope. This is particularly true for the 1085 cm^{-1} map where IR absorption closely tracks the AFM images. Presumably this is due to the contribution from phospholipid headgroups being dominant in the unexposed cell. After exposure, the spatial correlation between absorption at 1085 cm^{-1} and AFM maps is lost, particularly at higher dose. The IR maps take on an irregular appearance, with loss of any discernible structure and overall absorbance increases. This is consistent with the accumulation of RNA following increased protein synthesis. RNA does not accumulate in such a way as to track cellular and nuclear topography, thus preventing recognition of nucleoli or other structures in IR maps. Maps at 1668 cm^{-1} are more complex, since they contain contributions from protein absorption from throughout the cell even before irradiation. Nonetheless, before irradiation absorption at 1668 cm^{-1} still tracks the topography of the nucleoli, presumably because of chromatin absorption. This structure is lost following irradiation, in agreement with the unstructured accumulation of newly synthesized proteins.

Concluding the infrared studies, we have shown that the Hyperion 3000/Vertex 70v unit at the laboratory for spectroscopic imaging can be used as a tool to study radiation exposure of cells and, by extension, tissue. Additional and complementary information about radiation damage at subcellular level can be provided by performing AFM-IR imaging with the nanoIR2 instrument. Analysis of the FTIR measurements via PCA provides clear clustering of samples based on the dose of radiation received. The classification can be ascribed to the changes in molecular composition induced by radiation exposure. The dose dependence of spectral properties creates the opportunity to develop classification models for cells exposure based on FTIR microspectroscopy, as already proposed by this laboratory [Lipiec 2014]. This would provide a tool for assessing exposure of individual cells in samples subject to non-homogeneous exposure, such as tissue undergoing micro-beam radiation treatment.

Raman spectroscopy.

The Raman band wavenumbers and the proposed band assignments, are given in Table 1. Application of the immersion objective enables measurements on live cells in a buffer.

Table 1. Wavenumbers and proposed band assignments for the Raman spectra of T24 cells, and these cells after irradiation of 3 Gy and 10 Gy, respectively.

wavenumbers [cm^{-1}]			Assignment[a]
T24	T24 3Gy	T24 10Gy	
2851	2850	2850	$\nu_s(CH_2)_{lipids}$
1657	1657	1657	$\nu(C=C)_{amide}$,$\nu(C=O)_{carbonyl}$, $\nu(C=C)_{cis,\ lipids,\ fatty\ acids}$
		1506	„ring–breathing" vibrations in the DNA bases: A, C
1481	1481	1481	$\delta(CH)_{lipids}$
1450	1452	1452	$\delta(CH_2)/(CH_3)/(CH)$
1337	1338	1339	$\rho_w(CH_3)/(CH_2)_{collagen,\ nucleic\ acids}$
1307	1305	1305	$\rho_t/\rho_w(CH_2)_{lipids,\ fatty\ acids}$
1250	1250	1250	$\nu_{as}(O–P–O)$
1234	1240	1240	$\nu_{as}(O–P–O)$
1194	1195	1195	$\nu(O\text{-}P\text{-}O)_{DNA\ backbone}$
1127	1125	1125	$\nu(C–C)_{skeletal\ of\ acyl\ backbone\ in\ lipids}$, $(C–N)_{proteins}$, $\nu(C–C)_{lipids,\ proteins}$
1092	1093	1093	$\nu_s(O\text{-}P\text{-}O)_{DNA\ backbone}$
1086		1086	$\nu_s(O\text{-}P\text{-}O)_{DNA\ backbone}$
1065	1066	1066	$\nu(C\text{-}O)_{DNA\ backbone}$
1031	1031	1031	$\nu(C\text{-}C)_{phenylalanine}$
1003	1003	1003	$\delta(C\text{-}C)_{phenylalanine}$
880	880	880	$\nu(C\text{-}O)_{DNA\ backbone}$

[a]Abbreviations:
ν, stretching; ρ_t, twisting; ρ_w, wagging; δ, deformation; s, symmetric; as, antisymmetric.

Figure 22 presents Raman spectra of the aforementioned cells together with the corresponding microscope images. As it is observed, Raman spectra of the reference T24 cells and these cells after irradiation indicate similarities in intensities and positions of the characteristic bands (see Table 1 for band assignment). However, some observed band shift and changes in relative intensities are associated with the irradiation. Briefly, essential changes in Raman band intensities appear at ~1195 cm^{-1} [ν(O-P-O) $_{backbone\ DNA}$], ~1065 cm^{-1} [ν(C-O)$_{backbone\ DNA}$], and ~880 cm^{-1} [ν(C-O)$_{backbone\ DNA}$], are due to strand breaks of the DNA chain and change in structure of the DNA sugar residue [*Chan 2006*, *Sailer 1996*]. Moreover, a band shift noticed for Raman band from 1234 cm^{-1} for reference cell line to ~1240 cm^{-1} for irradiated 3 Gy and 10 Gy cells, respectively, suggests that after irradiation the partially changes of the DNA conformation from B–DNA to A–DNA form, occur [*Sailer 1996*]. On the other hand, the observed changes in lipid regions may be associated with changes taking place in their structure upon irradiation [*Gniadecka 1997*].

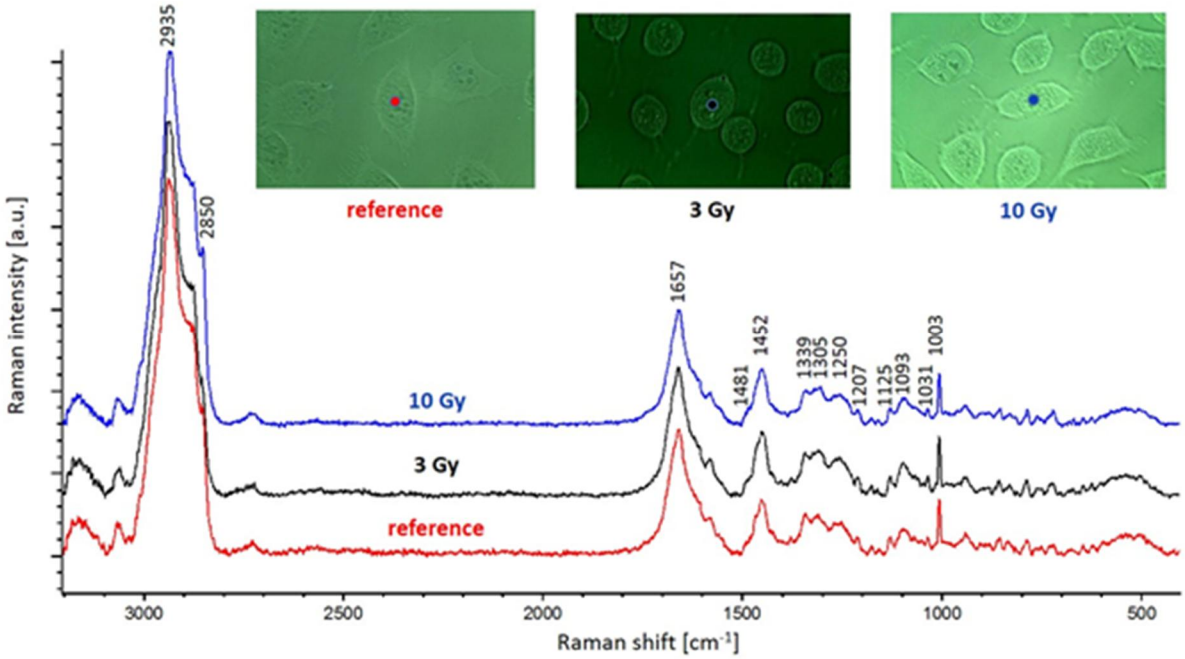

Figure 22. *Raman spectra of the live T24 cells and these cells after 3 Gy and 10 Gy irradiation together with the microscope images.*

Figure 23 shows the Raman spectra of the fixed T24 cells (reference) and these cells after 3 Gy and 10 Gy irradiation together with the corresponding microscope images. As it was noticed for the live T24 cells, Raman spectra of the fixed cells are similar, but show some band shifts and changes in relative intensities. In the high wavenumber region, Raman spectrum of 10 Gy dose shows slightly different pattern (*e.g.* shoulder band at ca. 2850 cm^{-1}) due to structural changes in lipids caused by the irradiation [*Gniadecka 1997*]. On the other hand, low wavenumber region shows some distinct differences between Raman spectra of reference, 3Gy, and 10 Gy samples. Firstly, in the Raman spectra of the investigated fixed cells after 10 Gy irradiation a band at ~1506 cm^{-1} appears, which can be associated with the „ring–breathing" vibrations in the DNA bases: A, C [*Chan 2006*]. The band is not observed in the Raman spectrum of 3 Gy dose. Furthermore, this band is absent in the Raman spectra of the T24 live cells after irradiation with the same dose (see Figure 22 and 24B).

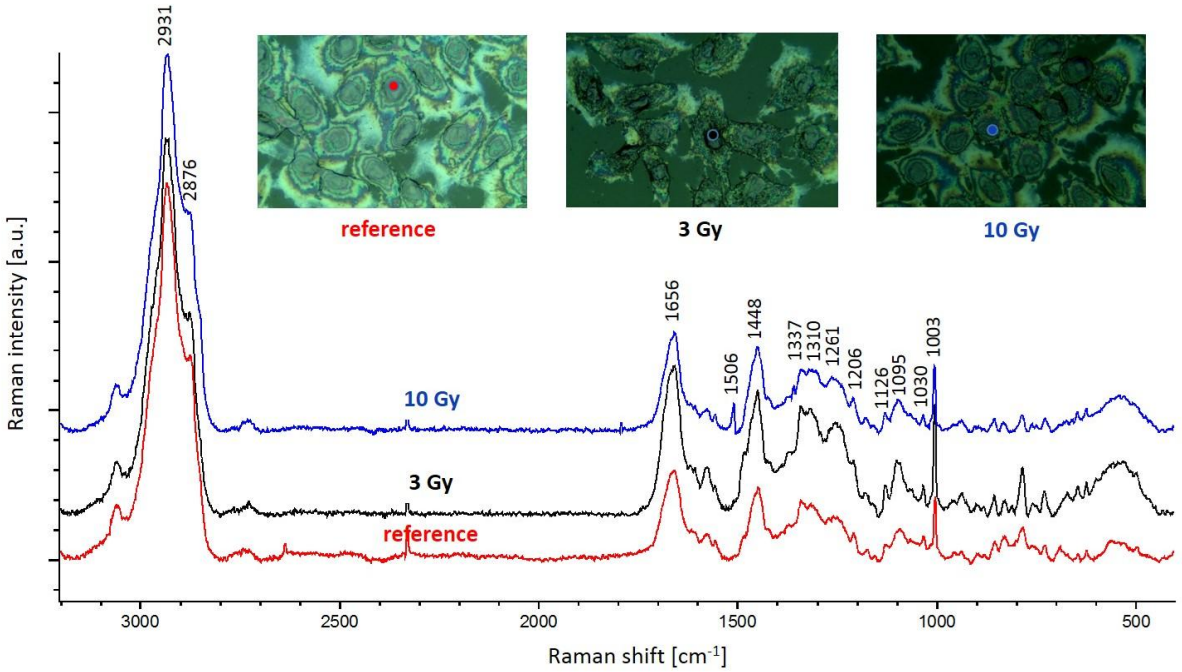

Figure 23. *Raman spectra of the fixed T24 cells and these cells after 10 Gy irradiation together with the microscope images.*

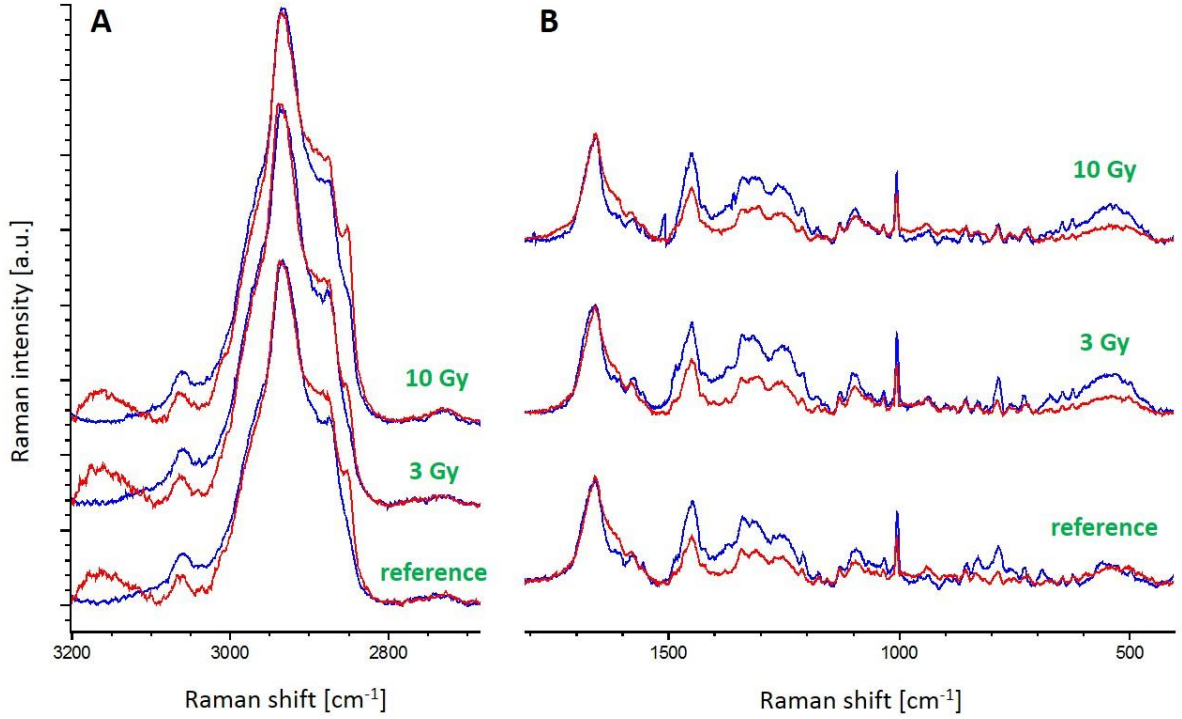

Figure 24. *Raman spectra of the live (red) and fixed (blue) T24 cells (reference) and these cells after 3 Gy and 10 Gy irradiation in the high wavenumber (A) and low wavenumber (B) regions.*

Secondly, the strand breaks of the DNA chain and changes in the structure of the DNA sugar residue and backbone upon irradiation, occur. This is manifested by observed intensity changes that appear at ~1575 cm^{-1}, ~1095 cm^{-1}, ~1065 cm^{-1}, ~880 cm^{-1}, and ~665 cm^{-1} as well as in the region of 1220 – 1280 cm^{-1} (see Table 1 for precise assignments) in Raman spectra of the fixed T24 cells and these cells after irradiation [*Chan 2006, Sailer 1996, Shetty 2006*]. On the other hand, Raman spectra of the fixed cells and these cells after irradiation (see Figure 23) show changes in intensities of the deformations of CH_3 and CH_2 observed at ~1337 cm^{-1} and ~1310 cm^{-1}, respectively [*Chan 2006, Gniadecka 1997*]. It indicates changes in the lipid structure upon irradiation.

Raman spectra of the live and fixed T24 cells differ from each other in both high and low wavenumber regions (Figure 3). The most distinct differences can be observed in the 2800 – 3200 cm^{-1} region (bands at ~2850 cm^{-1} and ~2875 cm^{-1} related to lipids as well as a band at ~3100 cm^{-1} corresponding to water). Furthermore, in the 500 – 1800 cm^{-1} region changes in relative band intensities can be clearly observed (Figure 3B). As can be seen, Raman signals observed in the 1200 – 1500 cm^{-1} region as well as a phenylalanine band (~1005 cm^{-1}) exhibit lower intensities in relation to the Amide I band (1657 cm^{-1}). Additionally, as it was mentioned above, Raman spectrum of fixed cells after 10 Gy irradiation shows a band at ~1506 cm^{-1}, which does not appear in the corresponding spectrum of live cells.

Complementary techniques: UV-VIS and PCR

Cytotoxic effect of X-ray was measured as presence of LDH level in culture medium (Figure 25). There was no statistic effect of incubation time on presence of membrane damage in non-irradiated cells (control). Significantly increased of damage cells after 1 Gy as well as after 3 Gy irradiation (*p < 0.0001 in comparison to non-irradiated cells) independently on time after irradiation was observed. The day after irradiation no additional increase of the cytotoxic effect in comparison to cytotoxicity after 1 hour was observed (no statistical effect of time culturing). Then the cell membranes damage and thereby necrotic death as a result of X-ray treatments (1 Gy and 3 Gy) appeared right after irradiation.

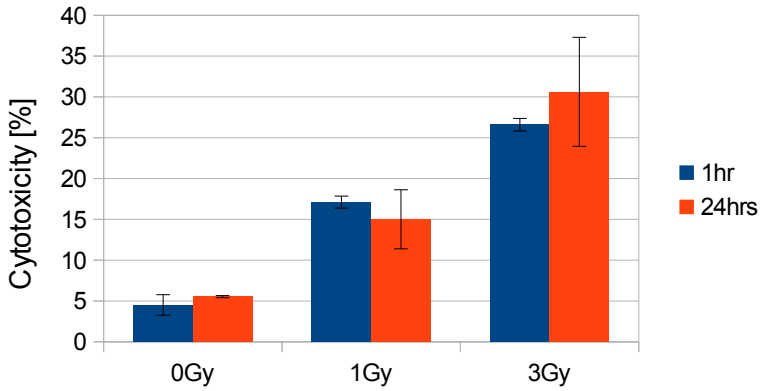

Figure 25. *Cytotoxic effect of X-ray on cells. Significant effect of irradiation (*p < 0.0001) in comparison to non-irradiated cells.*

On the basis of γ-H2AX test, the fluorescence related to presence of double strand breaks in DNA (DSBs) in 1st and 2nd day of culture (1 hour and 24 hours after irradiation) was analyzed (Figures 26, 27).

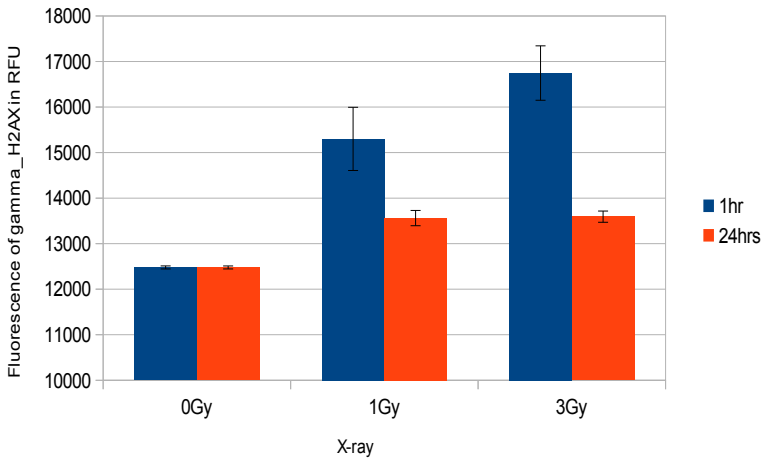

Figure 26. *Fluorescence level of γ-H2AX in cells irradiated (arbitrary absolute units).*

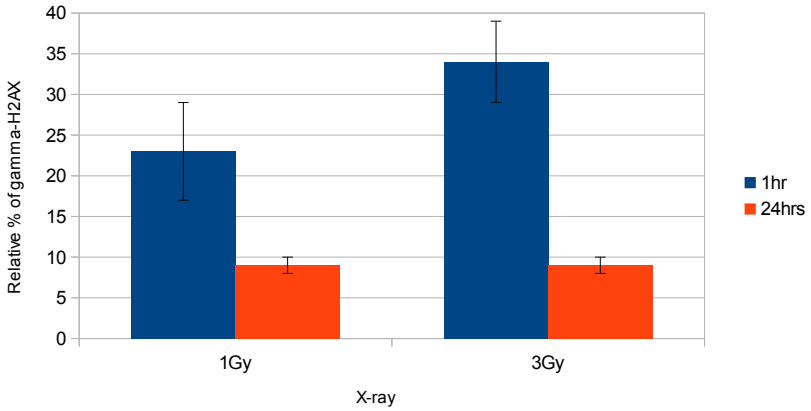

Figure 27. *Percentage of γ-H2AX expressed after X-ray related to control (non-treated cells).*

There was no statistic effect of incubation time on presence of DSBs in non-irradiated cells (control). The DSBs statistically increased in irradiated cells in comparison to non-irradiated cells, as expected [Kuo 2008]. The increase of DSBs in dependency on doses was observed in 1 hour of post-irradiation incubation ($p < 0.003$). Independent on dosages, the DSBs remained constant after 24 hours of irradiation and they were still higher than in control group ($p < 0.01$). That suggested that the repair processes of DNA have not been finished yet or death processes (e.g. apoptosis) have been initiated [Cleaver 2011, Watters 2009].

As mentioned above the RT-PCR system for real-time testing of DNA sequence was used in gene expression studies. Basing on the standard curves presented on Fig. 13, the number of gene copies in the wells of unknown concentration were estimated. The following results were obtained for individual blocks:

Table 2. *Fast 96 Well Block:*

Sample	Target	Quantity (Mean)	Quantity (Std Dev)	C_T (Mean)	C_T (Mean)
10K	RNase P	9,893.323	435.079	27.191	0.060
5K	RNase P	4,851.096	277.751	28.172	0.078

Table 3. *384 Well Block:*

Sample	Target	Quantity (Mean)	Quantity (Std Dev)	C_T (Mean)	C_T (Mean)
10K	RNase P	9,517.513	405.467	27.239	0.050
5K	RNase P	5,011.201	258.816	28.145	0.073

From the obtained results it was found that the test samples on each plate contained the 5000 or 10000 copies of the gene RNAse P.

Conclusions

The presented results demonstrated that the AFM elasticity measurements can be applied to quantitatively estimate alterations induced upon X-ray irradiation at the single cell level.

We have shown that the nanoIR2 unit can be used to characterize molecular changes occurring in the nuclear environment following cellular irradiation. The most accessible information is the change in distribution of macromolecules with a spatial resolution at the level of the single organelle. We show that changes in several spectroscopic ranges correlate with radiation dose and provide a tool for studying the biological effects of radiation exposure.

We have also shown that the Hyperion 3000/Vertex 70v unit at the laboratory for spectroscopic imaging can be used as tool to study radiation exposure of cells and, by extension, tissue. The classification can be ascribed to the changes in molecular composition induced by radiation exposure. Analysis of the measurements via PCA provides clear clustering of samples based on the dose of radiation received. The dose dependence of spectral properties creates the opportunity to develop classification models for cells exposure based on FTIR microspectroscopy, as already proposed by this laboratory. This would provide a tool for assessing exposure of individual cells in samples subject to non-homogeneous exposure, such as tissue undergoing micro-beam radiation treatment.

The application of Raman microspectroscopy for radiation-induced damage investigations provide detection of such spectral changes as strand breaks, base unstacking, and DNA conformational transformations. These studies give crucial information about the damage associated with irradiation and cellular response for radiation dose at single cell level. Moreover, this spectroscopy method provides possibility to investigate structural changes present within the same sample.

The complementary techniques such as UV-VIS and PCR provide specific information on the biological response to the radiation and shade additional view on spectroscopic imaging.

Acknowledgement

The research has been carried out in Laboratory of spectroscopic imaging for radiobiology, treatment and research of complex systems at the Institute of Nuclear Physics, Polish Academy of Sciences in Krakow under the project co-funded by the Malopolska Regional Operational Program Measure 5.1 Krakow Metropolitan Area as an important hub of the European Research Area for 2007-2013.

References

- [Adjei 2015] DanielAdjei, Mesfin Getachew Ayele, Przemyslaw Wachulak, Andrzej Bartnik, Łukasz Wegrzynski, Henryk Fiedorowicz, Luděk Vyšín, Anna Wiechec, Janusz Lekki, Wojciech M. Kwiatek, Ladislav Pina, Marie Davídková, Libor Juha, "Development of a compact laser-produced plasma soft X-ray source for radiobiology experiments", *Nuclear Instruments and Methods in Physics Research Section B*, Volume **364**, 1 (2015) 27-32.

- [Bożek 2009] S. Bożek, J. Bielecki, J. Baszak, H. Doruch, R. Hajduk, J. Lekki, Z. Stachura, W.M. Kwiatek, "X-ray microprobe – a new facility for cell irradiations in Kraków", *Nucl. Instr. Meth. in Phys. Res.* B **267** (2009) 2273–2276.

- [Chan 2006] Chan, J. W., Taylor, D. S., Zwerdling, T., Lane, S. T., Ihara, K. & Huser, T. Micro–Raman spectroscopy detects individual neoplastic and normal hematopoietic cells. Biophys J. **90** (2006) 648–656.

- [Criswell 2003] Criswell, T; Leskov, K; Miyamoto, S; Luo, GB; Boothman, DA;Oncogene, 2003, Volume: 22, Issue: 37, Pages: 5813-5827.

- [Folkard 2001] M. Folkard et al., The impact of microbeams in radiation biology, Nucl. Instr. Meth. B **181** (2001) 426.

- [Folkard 2006] M. Folkard, K.D. Atkinson, G. Flaccavento, P.R. Barber, R.J. Locke, G. Pierce, S. Gilchrist, A.G. Michette, K.M. Prise, B. Vojnovic, "Development of the GCI Multi-target X-Ray Microprobe", Radiation Research, **166** (4) (2006) pages 659-660.

- [Gerardi 2006] S. Gerardi, "A comparative review of the charged particle microbeam facilities", Radiat. Prot. Dos., 122 (2006) 285.

- [Gniadecka 1997] Gniadecka, M., Wulf, H. C., Mortensen, N. N., Nielsen, O. F. & Christensen, D. H. Diagnosis of basal cell carcinoma by Raman spectroscopy. J. Raman Spectr. **28** (1997) 125–129.

- [Imaseki 2007] H. Imaseki, T. Ishikawa, H. Iso, T. Konishi, N. Suya, T. Hamano, X. Wang, N. Yasuda, M. Yukawa, "Progress report of the single particle irradiation system to cell (SPICE)", Nucl. Instr. and Meth. B **260** (2007) 81–84.

- [Kuo 2008] Kuo L. J. and Yang Li-Xi, γ-H2AX – A Novel Biomarker for DNA Double-strand Breaks, In Vivo *22* (2008) 305-310. [Cleaver 2011] Cleaver JE, H2AX: Biomarker of damage or functional participant in DNA repair ''All that Glitters Is not Gold!". Photochem Photobiol.**87** (2011) 1230–1239.

- [LDH 2007] LDH Cytotoxicity Detection Kit User Manual; online: www.clontech.com; 2007

- [Lekka 1999] Lekka M, Laidler P, Gil D, Lekki J, Stachura Z, Hrynkiewicz AZ, Elasticity of normal and cancerous human bladder cells studied by scanning force microscopy. Eur. Biophys J **28** (1999) 312-316.

- [Lekka 2012] Lekka, M., Gil, D., Pogoda, K., Dulińska-Litewka, J., Jach, R., Gostek, J., Klymenko, O., Prauzner-Bechcicki, S., Stachura, Z., Wiltowska-Zuber, J., Okoń, K., and Laidler, P., Cancer cell detection in tissue sections using AFM. Arch. Biochem. Biophys. **518** (2012) 151–6.

- [Lekki 2014] J. Lekki, J. Bielecki, S. Bożek and Z. Stachura, „Application of Focused X-ray Beams in Radiation Biology" in Short Wavelength Laboratory Sources: Principles and Practices, Royal Society of Chemistry, 2014, Eds: Davide Bleiner, John Costello, Francois Dortan, Gerry O'Sullivan, Ladislav Pina, Alan Michette, ISBN: 978-1-84973-456-1, p. 381–397.

- [Lipiec 2014] Lipiec, Ewelina; Bambery, Keith R.; Heraud, Phil; et al. JOURNAL OF MOLECULAR STRUCTURE, Volume: **1073** (2014) 134-141.

- [Lipiec 2015] E. Lipiec, K. R. Bambery, J. Lekki, M. J. Tobin, C. Vogel, D. R. Whelan, B. R. Woodd and W. M. Kwiatek, "SR-FTIR Coupled with Principal Component Analysis Shows Evidence for the Cellular Bystander Effect", *Radiat Res.* **184** (1) (2015) 73-82.

- [Nagasawa 1999] H. Nagasawa, J.B. Little, "Unexpected sensitivity to the induction of mutations by very low doses of alpha-particle radiation: Evidence for a bystander effect", Radiat. Res. **152** (1999) 552.

- [Nikjoo 1998] H.Nikjoo et al., "Track structure in radiation biology: theory and applications", Int. J. Rad. Biol., **73** (1998) 35.5.

- [Nuta 2008] O. Nuta, F. Darroudi, "The impact of the bystander effect on the low-dose hypersensitivity phenomenon", Radiat Environ. Biophys. **47** (2008) 265–274.

- [Sader 1999] Sader, J.E., Chon, J.W.M., and Mulvaney, P., Calibration of rectangular atomic force microscope cantilevers. Rev. Sci. Instrum. **70** (1999)3967–3969.

- [Sailer 1996] Sailer, K., Viaggi, S. & Nusse, M. Radiation–induced structural modifications in dsDNA analysed by FT–Raman spectroscopy. Int. J. Radiat. Biol. **69** (1996) 601–613.

- [Shetty 2006] Shetty, G., Kedall, C., Shepherd, N., Stone, N., & Barr, H., Raman spectroscopy: Evaluation of biochemical changes in carcinogenesis of oesophagus. Br. J. Cancer. **94** (2006) 1460–1464.

- [Tubiana 2005] M. Tubiana, A. Aurengo, D. Averbeck, A. Bonnin, B. Le Guen, R. Masse, R. Monier, AJ. Valleron, and F. de Vathaire, Joint Report n° 2, Academie Nationale de Medecine, Institut de France—Academie des Sciences, "Dose–effect relation-ships and the estimation of the carcinogenic effects of low doses of ionizing radiation". Edition Nucleon (Paris 2005) ISBN 2-84332-018-617, (http://www.academiemedecine.fr/actualites/rapports.asp).

- [Ugenskiene 2007] R. Ugenskiene, J. Lekki, W. Polak, K. Prise, M. Folkard, O. Veselov, Z. Stachura, W.M. Kwiatek, M. Zazula, and J. Stachura, Double strand break formation as a response to X–ray and targeted proton irradiation, Nucl. Instr. and Meth. in Phys. Res. B. **260** (2007) 159–163.

- [Watters 2009] Watters GP, Smart DJ, Harvey JS, Austin CA. H2AX phosphorylation as a genoticity endpoint. Mutat Res. **679** (2009) 50–58.